CrossMark

RESEARCH PAPER

Nanojoining of crossed Ag nanowires: a molecular dynamics study

**Jianlei Cui · Xuewen Wang ·
Theogene Barayavuga · Xuesong Mei ·
Wenjun Wang · Xiaoqiao He**

Abstract Ag nanowires are considered to be the promising candidates for future electronic circuit owing to the excellent electrical and thermal properties, with the miniaturization of electronics devices into nanometer scale. Though interconnect technology between Ag nanowires (Ag NWs) is essential for nanofunctional devices, it lacks sufficient experimental data. Besides, the determination of Ag NW interconnection configuration is experimentally difficult to do for lacking the sufficient investigation of atomic configuration evolution during nanojoining process. So the nanojoining between the crossed Ag NWs with the same diameter of 2 nm and different lengths was performed by molecular dynamics simulation to explain the unclear nanojoining mechanism based on thermal effect. As the simulation results present, when the nanojoining temperature is relatively high, though the Ag NWs are connected with the interpenetration effect of Ag atoms at the crossed nanojunction area, the nanostructures of Ag NWs have been seriously deformed with shorter length and larger diameter, showing relatively more obvious melting characteristics based on the chaotic atomic structures. If the temperature is reduced to 300 K as cold welding, the crossed Ag NWs can be partially contacted with the partial mixture of Ag atoms, and the interstices always exist between the Si surface and the upper Ag nanowire. In addition, the obvious dislocation phenomenon will appear and evolve as time goes on. Consequently, the dominant mechanism was revealed for providing a fundamental understanding of how 'hot' and 'cold' welding technology affects the atomic contact configuration, respectively.

Keywords Nanojoining · Ag nanowires · Atomic configuration · Molecular dynamics · Modeling and simulations

J. Cui · X. Wang · T. Barayavuga · X. Mei · W. Wang
State Key Laboratory for Manufacturing Systems
Engineering, Xi'an Jiaotong University, Xi'an 710049,
People's Republic of China

J. Cui · X. Wang · T. Barayavuga
State Key Laboratory of High Performance Complex
Manufacturing, Central South University,
Changsha 410083, People's Republic of China

J. Cui
State Key Laboratory of Advanced Welding and Joining,
Harbin Institute of Technology, Harbin 150001, People's
Republic of China

J. Cui (✉) · X. He (✉)
Department of Architecture and Civil Engineering, City
University of Hong Kong, Tat Chee Avenue, Kowloon,
Hong Kong
e-mail: cjlxjtu@mail.xjtu.edu.cn

X. He
e-mail: bcxqhe@cityu.edu.hk

2 Springer

Introduction

With the development of nanoscience and nanotechnology, the 'Top–Down' approach has been used to etch small integrated circuit structures for the pursuit of low weight, high speed and other good performances. However, the inability to etch nanostructures by laser with the shorter wavelength has limited how precisely they can design and fabricate nanocircuits on semiconductor material (ITRS 2013). For fabricating nanoelectronic devices, the 'Bottom–Up' processes, such as self-assembly, aggregation, or adsorption, are becoming increasingly popular.

The transition metal nanowires are selected as the bridge between nanodevice performances, such as Ag, Au, etc. Considering the excellent electrical and thermal properties, the Ag NWs are considered to be the promising candidates for future electronic circuit. The interconnect technology of Ag NWs will become a prerequisite for the next generation of nanodevices (van de Groep et al. 2012; Curto et al. 2013; Kim et al. 2013). For getting the excellent nanojoining quality between Ag NWs, many innovative microelectronics technologies were directly applied to interconnection, such as fusion welding (Kim and Jang 2005; Xu et al. 2005; Tohmyoh et al. 2007; Cui et al. 2015), brazing (Dockendorf et al. 2007; Wu et al. 2008; Peng et al. 2008), and solid-phase bonding (Duan et al. 2005; Chen et al. 2006; Shen et al. 2009; Guo 2010). According to the latest research progress, the Ag NW and Ag NW can be well connected experimentally with cold welding technology (Lu et al. 2010). And the light-induced self-limited plasmonic welding method of Ag NW junctions was experimentally performed (Garnett et al. 2012). The effective and promising nanojoining technologies were mainly used to join nanowires aiming at the common crossed Ag NWs junctions, experimentally.

Unfortunately, the nanojoining technology lacks sufficient experimental data, and the determination of structures of Ag NWs interconnection is difficult to be verified because of the unclear nanojoining mechanism. However, molecular dynamics (MD) simulation provides a powerful method to investigate the structural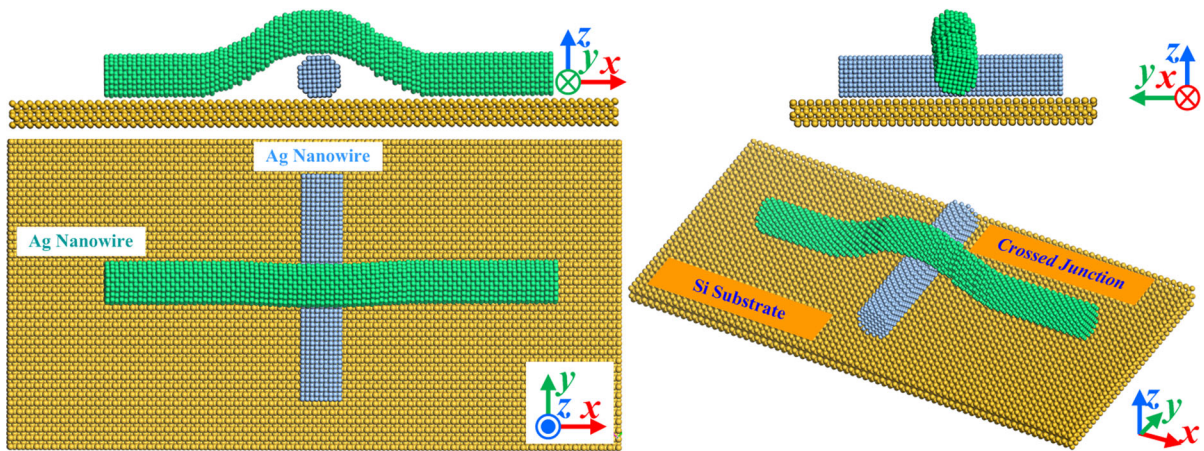 and dynamical properties in a realistic manner (Cui et al. 2013a, b, c, 2014a, b; Pereira and Da Silva 2011; Guo et al. 2012). Consequently, for revealing the dominant mechanism and providing a fundamental understanding of how 'hot' and 'cold' welding technology, respectively, affects the atomic contact configuration, the detailed nanojoining process of the crossed Ag nanowires was simulated as the main research objective in this paper.

Computational methodology

Figure 1 presents the atomic structural model of the crossed Ag NWs on the [1 0 0] plane of Si substrate. For getting accurate and effective physical data to reveal the nanojoining mechanism, the key of MD simulation is the selection of the interatomic force field, which determines the work load, accuracy of simulation results, and the degree of approximation between the calculation model and the real system. So the powerful COMPASS (Condensed-phase Optimized Molecular Potentials for Atomistic Simulation Studies) force field, as a parameterized, tested and validated first ab initio force field, was selected in the MD simulation of nanojoining process, which enables an accurate prediction of condensed matter physics (Sun 1994, 1998; Cui et al. 2013a, b, c, 2014a, b; Yan et al. 2009). In the COMPASS force field, the total potential energy of system includes the valence terms and non-bonded interaction terms, and the valence terms are composed of diagonal term E_{bond} and off-diagonal cross-coupling term E_{cross}, which are given by the following functions.

$$
\begin{aligned}
E_{total} &= E_{valence} + E_{non-bond} \\
&= E_{bond} + E_{cross} + E_{non-bond}
\end{aligned} \quad (1)
$$

$$
\begin{aligned}
E_{bond} &= E_b + E_\theta + E_\phi + E_\chi \\
&= \sum_b \left[K_2(b-b_0)^2 + K_3(b-b_0)^3 + K_4(b-b_0)^4 \right] \\
&+ \sum_\theta \left[H_2(\theta-\theta_0)^2 + H_3(\theta-\theta_0)^3 + H_4(\theta-\theta_0)^4 \right] \\
&+ \sum_\phi \left[V_1(1-\cos\phi) + V_2(1-\cos 2\phi) \right. \\
&\left. + V_3(1-\cos 3\phi) \right] + \sum_\chi K_\chi(\chi-\chi_0)^2
\end{aligned} \quad (2)
$$

Fig. 1 Different atomic structural views for nanojoining process of the crossed Ag nanowires

$$E_{cross} = E_{bb'} + E_{b\theta} + E_{b\phi} + E_{\theta\theta'} + E_{\theta\theta'\phi}$$

$$= \sum_{b,b'} F_{b,b'}(b-b_0)(b'-b_0')$$

$$+ \sum_{b,\theta} F_{b,\theta}(b-b_0)(\theta-\theta_0) + \sum_{b,\phi}(b-b_0)$$

$$\times \left[F_{b,\phi}^{(1)}(1-\cos\phi) + F_{b,\phi}^{(2)}(1-2\cos\phi) \right.$$

$$\left. + F_{b,\phi}^{(3)}(1-3\cos\phi) \right]$$

$$+ \sum_{\theta,\theta'} F_{\theta,\theta'}(\theta-\theta_0)(\theta'-\theta_0')$$

$$+ \sum_{\theta,\theta'\phi} F_{\theta,\theta'\phi}(\theta-\theta_0)(\theta'-\theta_0')\cos\phi$$

$$\tag{3}$$

$$E_{non-bond} = E_{LJ} + E_{elec}$$

$$= \sum_{i,j} \varepsilon_{ij} \left[2\left(\frac{\sigma_{ij}^0}{r_{ij}}\right)^9 - 3\left(\frac{\sigma_{ij}^0}{r_{ij}}\right)^6 \right] + \sum_{i,j} \frac{q_i q_j}{\varepsilon_0 r_{ij}}$$

$$\tag{4}$$

here E_b, E_θ, E_ϕ, and E_χ represents bond, angle, torsion, and out-of-plane angle coordinates, and $E_{bb'}$, $E_{b\theta}$, $E_{b\phi}$, $E_{\theta\theta'}$, and $E_{\theta\theta'\phi}$ give cross-coupling term between internal coordinates, respectively. The non-bonded term $E_{non-bond}$ includes Lennard–Jones (LJ) 9–6 potential function for the vdW interaction E_{LJ} and a Coulomb term for electrostatic interactions. And it is used for interaction between pairs of atoms that are separated by three or more intervening atoms, or those that belong to different molecules. Thereinto, the LJ

potential parameters are listed in Table 1, and the ε represents the bonding strength between atoms and σ gives the atomic interaction radius (Timpel et al. 1997).

Results and discussion

In the MD simulation, the nanojoining process was performed under the constant NVT ensemble with the Andersen thermostat. The initial velocities of all atoms were set as Maxwell–Boltzmann distribution, and the Velocity Verlet was selected as integration method. Taking into account the nanojoining simulation that aims to explore contact behavior of Ag NWs and interfacial characteristics based on the nanometer size effect, the positions of all Si atoms were constrained in the x, y and z direction based on the characteristics of macro silicon substrate material. And non-period boundary conditions were imposed on the three directions of the total simulation system due to the size effect of Ag NWs with the diameter of 2 nm.

Table 1 Sets of Lennard–Jones (LJ) potential parameters

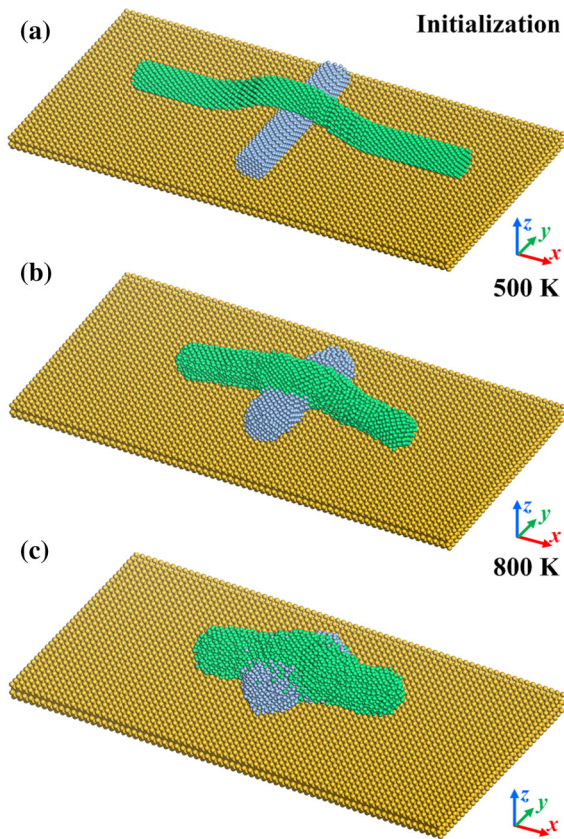|	Ag–Ag	Ag–Si
ε (eV)	0.3446	0.1498
σ (nm)	0.254	0.1917

During the simulation process of nanojoining, the atomic configuration and energy should be equilibrated to a stable state for getting accurate atomic physical information. So Fig. 2 gives the potential energy evolution of the total system with the simulation time of 1 ns at the different temperatures. The result shows that the fluctuation depends on temperature. Larger energy fluctuation exists at the higher temperature and vice versa. This is because the initial Ag atoms are applied at the high random velocities in the thermostat with high temperature, and more vigorous movement appears subsequently. The average atomic volume increases based on the vigorous movement, which causes the dramatical augment of potential energy. However, as for the potential energy, it needs to take a long time to fall for keeping the minimization of system energy. So the simulation system will also take a long time to reach the steady state for obtaining the final accurate atomic configurations with the interaction of the atoms. Namely, at the lower temperature, the potential energy will quickly achieve the stable state with small fluctuation from the relatively earlier simulation time. And the potential energy takes about 450 ps to reach approximate equilibrium state at the higher temperature of 800 K. From the stable equilibrium state of potential energy in Fig. 2, the values of potential energy seem to be close at the relatively lower and higher temperatures. But, based on the average atomic volume at the different temperature, the final stable potential energy subsequently increases as the temperature rises. Then, the final accurate atomic configuration can be got in
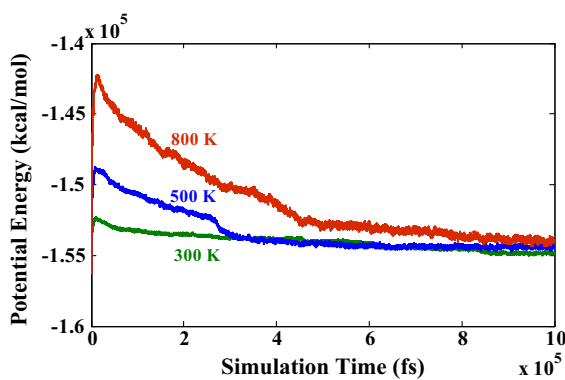
the stable condition at different temperatures. Considering the nanojoining temperature, the simulation time was set to 1 ns during the nanojoining process of the crossed Ag NWs.

For studying the 'hot' nanowelding between the crossed Ag NWs, Fig. 3 firstly displays the final atomic configurations with the simulation time of 1 ns at the different temperatures. As the initial atomic configuration, the two nanowires have the perfect crossed configuration without nanojoining operation. Increasing the nanojoining temperature to 500 K and 800 K, the corresponding final atomic configurations were got with achieving the nanointerconnect operation between nanowires. As the atomic configuration at the temperature of 500 K, the Ag NWs nanoconnection quality is relatively perfect with keeping its shape. By contrast, at the temperature of 800 K, although the Ag NWs are connected with the diffusion effect of Ag atoms at the crossed area, the nanostructures of Ag NWs have been seriously deformed with shorter length and larger diameter, showing relatively obvious melting characteristics with the chaotic atomic structures based on our previous researches (Cui et al. 2013a, b, c, 2014a, b). For studying the thermodynamical behavior of Ag atoms in detail, Fig. 4 shows the different atomic configurations at the different simulation times. At the shorter time of 10 ps, Ag NWs maintain good overall 1-D structures with larger length and smaller diameter. The two Ag NWs are connected together through the interaction and interpenetration of Ag NWs between lower part of upper nanowire and upper part of lower nanowire. At the same time, the larger interstice exists between the upper nanowire and lower nanowire. As time goes on, the interstice gradually becomes small, which mainly depends on the motion direction of Ag atoms of the upper Ag NW. And during the nanojoining process of the crossed Ag NWs, the Ag atoms of the upper Ag NW at the position of the interstice can be subjected to the interactive forces from the Si atoms of substrate and the Ag atoms of the lower Ag NW. Then, some Ag atoms can move toward the substrate surface, and they also lead to the downward movement of the neighboring Ag atoms due to the strong effect of metal bonds, with the interstice becoming smaller. In addition, with diffusion effect of Ag atoms at the crossed junction, the contact area gradually increases, comparing the small contact area at the relatively earlier simulation time. As the final atomic

Fig. 2 Potential energy evolution of the total system with simulation time at the different temperature during nanojoining process with 1 ns

Fig. 3 Time-averaged nanojoining configurations of the crossed Ag nanowires with the simulation time of 1 ns at the different temperature

$$\rho g(r) = N^{-1} \left[\sum_{i \neq j} \delta(r + R_i - R_j) \right] \qquad (5)$$

where ρ is the average density of the system, r represents the distance between atoms, δ gives the Dirac delta function, and N is the total number of atoms. And $g(r)$ reflects the distribution of an atom surrounded by other atoms, which is the probability of another atom found within the spatial extent of radius $r + \delta(r)$ when an atom is identified as the center. In the nanojoining simulations, at the temperature of 300 K, the RDF curve has the highest and most sharp peaks, which indicates the Ag NWs are in the solid state. When the temperature increases to 500 K, each peak of RDF curve is relatively high and sharp and the atomic arrangement of surface Ag atoms is not regular, which shows that the Ag NWs may be in the premelting state of surface structures and the solid state of internal structures, accompanying that Ag atoms vibrate and rotate near the balance position under the role of metal bonds with volume expansion of Ag NWs. So the Ag NWs as a whole show the characteristics of solid state. Increased to 800 K, the peaks of the RDF curve are gradually wakened and disappear while the grooves are filled to tend to the straight line direction, indicating that the Ag NWs have melted in the liquid state. So, as the final atomic configuration in Fig. 4c shows, the Ag NWs are in the melting state. If the adhesive force is ignored, with the effect of surface tension, the two Ag NWs will melt and form a similar circular structure in accordance with the behavior trends of the all Ag atoms. And even considering the effect of adhesion between Ag NWs and Si substrate, the similar circular configuration is also easily formed at the higher temperature, such as 1000 K. Consequently, the high temperature is not suitable for nanojoining process.

To solve the problems caused by high temperature, the nanojoining temperature should be reduced. For studying the nanojoining characteristics and 'cold' welding at the lower temperature, the evolution of atomic configuration was performed at 300 K in Fig. 6. Overall, as the atomic configurations of crossed Ag NWs during nanojoining, the lower blue Ag nanowire was almost unchanged practically. By comparison, the atomic structures of upper green nanowire changed obviously. As is shown by the nanojoining simulation of the initial atomic

configuration at 1 ns, the upper and lower Ag NWs are nearly in the same plane. So the quality of connection region is becoming better as time goes on, but with the defect of self-appearance of Ag NWs. When the time is 1 ns, the final atomic configuration is formed. The interstice disappears and the nanowires have been seriously deformed in Fig. 4c. Then, combining the final configuration formation phenomenon and the irregular structures of surface atoms, it indicates that the Ag NWs are in the molten state, showing the obvious flow and wetting characteristics.
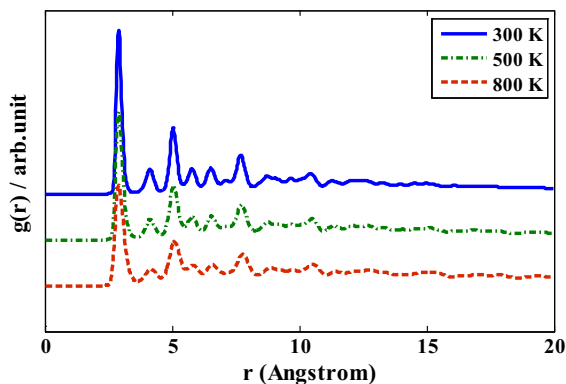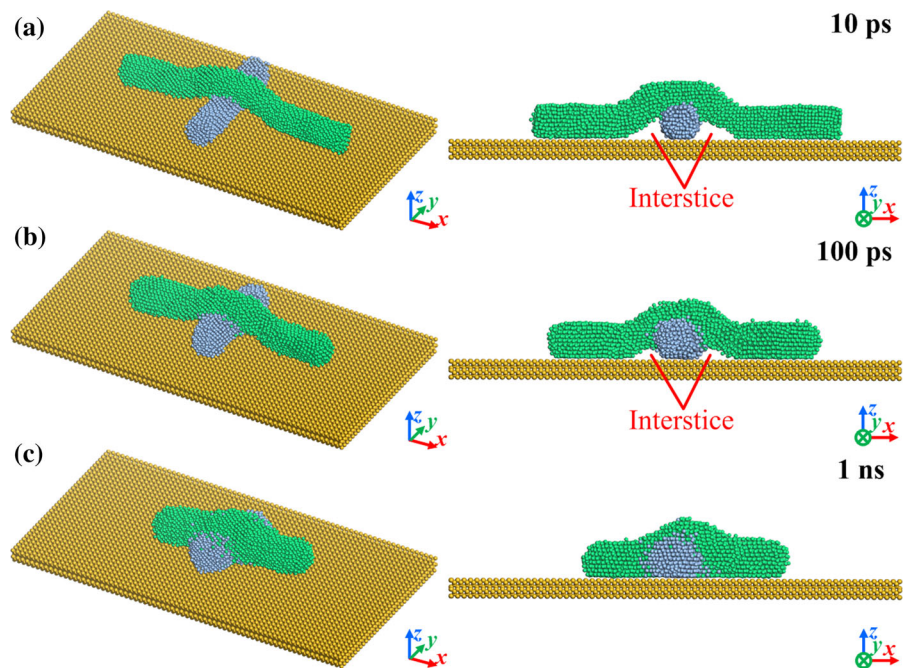
To further study the effect of temperature on the nanojoining and discuss the thermodynamical behavior of Ag NWs, Fig. 5 gives the radial distribution function (RDF) curves of the crossed Ag NWs at the different temperatures, which is widely used to describe the structural characteristics of liquid and amorphous state and it is defined as:

Fig. 4 Snapshots for instantaneous configurations of the crossed Ag nanowires with the simulation time of 1 ns at the temperature of 800 K


Fig. 5 Radial distribution function curves of the crossed Ag nanowires at different temperature

configuration in Fig. 1, at the time of 10–100 ps, the upper green nanowire structures become more compact toward the vertical blue nanowire due to the interaction of the two Ag nanowires, which also depends on metal bonds effect of all atoms to minimize the energy of the system. However, when the simulation time is 200, 500 ps and 1 ns, the total length of upper nanowire was further reduced, accompanying that the left half is shorter and thicker than the right half in surface profile, primarily because the spatial position of the two Ag NWs is not strictly

symmetrical and small distance changes will affect the Van der Waals force between atoms, going with changing the motion of atoms and showing different morphologies.

In order to further investigate the formation and characteristics of nanojunction of the crossed Ag NWs during the nanojoining process, Fig. 7 represents the instantaneous atomic configurations in x–z plane. At the low temperature of 300 K, the two nanowires are well connected as time goes on, and the interstices gradually become smaller. In addition, because the thermal motion and diffusion of atoms are weak at the low temperature, the interstices always exist between the Si surface and the upper Ag nanowire, and the two nanowires are partially contacted with partial mixture of Ag atoms, which is different from the nanojoining atomic configuration at the high temperature in Fig. 4c. During the nanojoining process, the profile of the left interstice is basically similar to the right part as the initial atomic configuration. However, the profile difference appears from 10 to 500 ps with similar morphologies of different sizes, such as the difference between the interstice in the red circle and the interstice in the red rectangle in Fig. 7f, the reason of which also lies in the effect of Van der Waals force induced by the spatial position of the atoms. And when

Fig. 6 Snapshots for instantaneous configurations of the crossed Ag nanowires with the simulation time of 1 ns at the temperature of 300 K
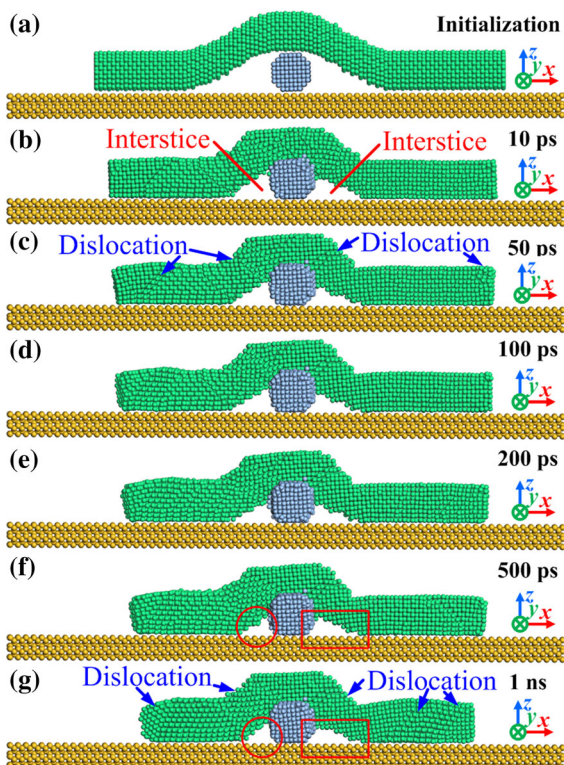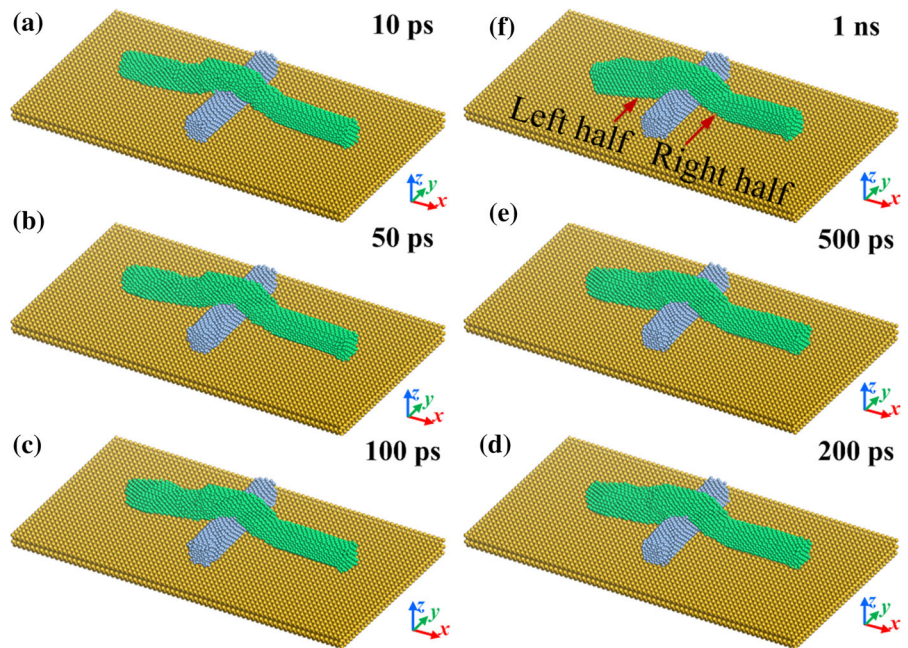
Fig. 7 Snapshots for instantaneous configurations (x–z plane) of the crossed Ag nanowires with the simulation time of 1 ns at the temperature of 300 K

the time is relatively long at 500 ps and 1 ns, the contour size no longer changes in the Fig. 7f and g, getting the final nanojoining atomic configuration. The phenomenon that Ag nanowires gradually become shorter and thicker can also be clearly seen from the nanojoining configurations in x–z plane. However, the obvious dislocation phenomenon appears at low temperature during nanojoining process, such as the dislocations in Fig. 7c. And over time, the dislocations will evolve with that in Fig. 7c changing into ones in Fig. 7g. The dislocation phenomenon is determined by the spatial position and thermal dynamic performance of atoms. As for the spatial position of the two Ag NWs, the interstice can provide more movement space for the Ag atoms of the upper nanowire. Subsequently, the nanojoining temperature empowers the Ag atoms to possess the strong thermal dynamic properties. With the strong effect of metal bonds at the same time, Ag atoms close to the central position can move a greater distance, comparing the initial and final atomic configurations. Due to the larger differences of displacements at the different positions, the dislocations always persist in the nanojoining process. All in all, the Ag NWs can be well connected with a small amount of dislocations at low temperature as cold welding. In addition, if we want to improve the nanojoining efficiency under the premise of getting the

quality of nanojunction, the interconnect temperature can be appropriately increased under premise of ensuring that the Ag NWs are not damaged.

Conclusions

The investigation of the nanojoining of the crossed Ag NWs was carried out using molecular dynamics simulation. Through the detailed atomic evolution configurations, the nanojoining process could be accomplished with different nanojunction characteristics at high and low temperature, respectively. When the nanojoining temperature is high, although the Ag NWs are connected with the diffusion effect of Ag atoms at the crossed nanojunction area, the nanostructures of Ag NWs have been seriously deformed with shorter length and larger diameter, showing relatively obvious melting characteristics based on the chaotic atomic structures. Thus, high temperature is not suitable for nanojoining. If the temperature is reduced to 300 K as cold welding, the crossed Ag NWs can be partially contacted with partial mixture of Ag atoms, and the interstices always exist between the Si surface and the upper Ag nanowire. In addition, the obvious dislocation phenomenon will appear and evolve as times go on. If we want to improve the nanojoining efficiency under the premise of getting the quality of nanojunction, the interconnect temperature can be appropriately increased, in the case of ensuring that the Ag NWs are not damaged. All in all, the Ag NWs can be well connected with a small amount of dislocations at low temperature as cold welding. And the elimination methods of dislocation need to be further studied for the better mechanical, thermal and electrical properties.

References

Chen C, Yan L, Kong ESW, Zhang Y (2006) Ultrasonic nanowelding of carbon nanotubes to metal electrodes. Nanotechnology 17:2192

Cui J, Yang L, Wang Y (2013a) Nanowelding configuration between carbon nanotubes in axial direction. Appl Surf Sci 264:713–717

Cui J, Yang L, Wang Y (2013b) Molecular dynamics study of the positioned single-walled carbon nanotubes with T-, X-, Y-junction during nanoscale soldering. Appl Surf Sci 284:392–396

Cui J, Yang L, Wang Y (2013c) Molecular dynamics simulation study of the melting of silver nanoparticles. Integr Ferroelectr 145:1–9

Cui J, Yang L, Zhou L, Wang Y (2014a) Nanoscale soldering of axially positioned single-walled carbon nanotubes: a molecular dynamics simulation study. ACS Appl Mater Interfaces 6:2044–2050

Cui J, Yang L, Wang Y (2014b) Size effect of melting of silver nanoparticles. Rare Met Mater Eng 43:369–374

Cui J, Yang L, Wang Y, Mei X, Wang W, Hou C (2015) Nanospot soldering polystyrene nanoparticles with an optical fiber probe laser irradiating a metallic AFM probe based on the near-field enhancement effect. ACS Appl Mater Interfaces 7:2294–2300

Curto AG, Taminiau TH, Volpe G, Kreuzer MP, Quidant R, van Hulst NF (2013) Multipolar radiation of quantum emitters with nanowire optical antennas. Nat Commun 4:1750

Dockendorf CPR, Steinlin M, Poulikakos D, Choi TY (2007) Individual carbon nanotube soldering with gold nanoink deposition. Appl Phys Lett 90:193116

Duan X, Zhang J, Ling X, Liu Z (2005) Nano-welding by scanning probe microscope. J Am Chem Soc 127:8268–8269

Garnett EC, Cai W, Cha JJ, Mahmood F, Connor ST, Christoforo MG, Cui Y, McGehee MD, Brongersma ML (2012) Self-limited plasmonic welding of silver nanowire junctions. Nat Mater 11:241–249

Guo S (2010) The creation of nanojunctions. Nanoscale 2:2521–2529

Guo JY, Xu CX, Hu AM, Shi ZL, Sheng FY, Dai J, Li ZH (2012) Welding of gold nanowires with different joining procedures. J Nanopart Res 14:1–12

Kim SJ, Jang DJ (2005) Laser-induced nanowelding of gold nanoparticles. Appl Phys Lett 86:033112

Kim A, Won Y, Woo K, Kim CH, Moon J (2013) Highly transparent low resistance ZnO/Ag nanowire/ZnO composite electrode for thin film solar cells. ACS Nano 7:1081–1091

Lu Y, Huang JY, Wang C, Sun S, Lou J (2010) Cold welding of ultrathin gold nanowires. Nat Nanotechnol 5:218–224

Peng Y, Cullis T, Inkson B (2008) Bottom–up nanoconstruction by the welding of individual metallic nanoobjects using nanoscale solder. Nano Lett 9:91–96

Pereira ZS, Da Silva EZ (2011) Cold welding of gold and silver nanowires: a molecular dynamics study. J Phys Chem C 115:22870–22876

Semiconductor Industry Association. International Technology Roadmap for Semiconductors (2013). http://public.itrs.net/

Shen G, Lu Y, Shen L, Zhang Y, Guo S (2009) Nondestructively creating nanojunctions by combined-dynamic-mode dip-pen nanolithography. ChemPhysChem 10:2226–2229

Sun H (1994) Force field for computation of conformational energies, structures, and vibrational frequencies of aromatic polyesters. J Comput Chem 15:752–768

Sun H (1998) COMPASS: an ab initio force-field optimized for condensed-phase applications overview with details on alkane and benzene compounds. J Phys Chem B 102:7338–7364

Timpel D, Scheerschmidt K, Garofalini SH (1997) Silver clustering in sodium silicate glasses: a molecular dynamics study. J Non-Cryst Solids 221:187–198

Tohmyoh H, Imaizumi T, Hayashi H, Saka M (2007) Welding of Pt nanowires by Joule heating. Scr Mater 57:953–956

van de Groep J, Spinelli P, Polman A (2012) Transparent conducting silver nanowire networks. Nano Lett 12:3138–3144

Wu W, Hu A, Li X, Wei J, Shu Q, Wang K, Yavuz M, Zhou Y (2008) Vacuum brazing of carbon nanotube bundles. Mater Lett 62:4486–4488

Xu S, Tian M, Wang J, Xu J, Redwing JM, Chan MHW (2005) Nanometer-scale modification and welding of silicon and metallic nanowires with a high-intensity electron beam. Small 1:1221–1229

Yan K, Xue Q, Xia D, Chen H, Xie J, Dong M (2009) The core/shell composite nanowires produced by self-scrolling carbon nanotubes onto copper nanowires. ACS Nano 3:2235–2240